E. BEŁTOWSKA-LEHMAN*, A. GÓRAL*, P. INDYKA*

ELECTRODEPOSITION AND CHARACTERIZATION OF Ni/Al$_2$O$_3$ NANOCOMPOSITE COATINGS

ELEKTROOSADZANIE I CHARAKTERYSTYKA NANOKOMPOZYTOWYCH POWŁOK Ni/Al$_2$O$_3$

The composite coatings containing of nanocrystalline Ni matrix and hard nano-sized γ-Al$_2$O$_3$ were electrodeposited in a system with a rotating disk electrode. The bath composition (nickel salts and buffer concentration, presence of surface-active agents and inert particles) influence on kinetics of Ni electrodeposition as well as on structural properties (morphology, phase composition, texture, residual stresses) and microhardness of Ni/Al$_2$O$_3$ coatings has been investigated. SEM and TEM studies show more uniform arrangement of Al$_2$O$_3$ particles in the matrix, however a tendency to agglomeration is observed. Surfactant application to a saccharine containing bath effectively improves the dispersion of nanoparticles into the nickel matrix. The addition of Al$_2$O$_3$ particles results in decrease of the average Ni crystallite size. The introduction of additive into electrolyte solution resulted in change of stress character of composite coatings (from tensile to compressive). The microhardness of Ni matrix was enhanced (about 40%) due to incorporation of ceramic particles.

Keywords: electrodeposition, nanocomposite, nickel coatings, Al$_2$O$_3$ nanoparticles

Nanokrystaliczne powłoki kompozytowe z osnową Ni zawierające ceramiczną fazę dyspersyjną w postaci γ-Al$_2$O$_3$ o rozmiarach nanometrycznych zostały elektroosadzone w układzie z wirującą elektrodą dyskową. W pracy analizowano wpływ składu kąpieli (zawartość soli niklu, obecność związków powierzchniowo-czynnych i cząstek obojętnych) na kinetykę procesu elektroosadzania, jak również na właściwości strukturalne (morfologię, skład fazowy, teksturę, naprężenia własne) oraz mikrotwardość powłok Ni/Al$_2$O$_3$. Badania wykonane za pomocą SEM i TEM wykazały, że cząstki Al$_2$O$_3$ są w znacznym stopniu równomiernie rozmieszczone w osnowie, jednak z tendencją do aglomeracji. Dodanie środka powierzchnio-czynnego do kąpieli zawierającej sacharynę zwiększyło dyspersję nanocząstek w osnowie niklu. Stwierdzono, że obecność cząstek Al$_2$O$_3$ powoduje obniżenie wielkości krystalitów osnowy Ni. Wprowadzenie dodatków do elektrolitu wpłynęło na zmianę charakteru naprężeń własnych uzyskanych powłok, jak również na ich mikrotwardość (wzrost o około 40%).

1. Introduction

Particle-reinforced metal matrix composite (MMC) coatings have found wide use in various engineering applications due to excellent mechanical properties compared to their components [1]. In composite materials, the metal matrix properties are modified by addition of various insoluble substances e.g. hard oxides as Al$_2$O$_3$, ZrO$_2$, SiO$_2$, carbides SiC and WC, diamond or solid lubricants (graphite, MoS$_2$ or PTFE) [2, 3]. The MMC structure allows to appear the interaction in phase boundary between the ductile matrix and embedded particles, which results in their specific characteristics differ from the component properties. The presence of ceramic particles could prevent migration of grain boundaries and dislocation movements resulting in enhanced thermal stability and hardness of MMC coating. The coatings demonstrate the metallic features (e.g. electric and thermal conductivity, plasticity) and the modifier properties (e.g. hardness, wear resistance). The composition and microstructure of electrodeposited composites control their functional properties, however the particles of suitable dimension must be uniformly dispersed to exhibit the dispersion-hardening effect.

Several metals, such as nickel, copper, chromium, gold, zinc, cobalt or alloys (e.g. Ni-Cu, Zn-Co, Co-Ni, Ni-Fe) were mainly used as a metallic matrix [4-7]. Among others nickel as a durable and tough metal has been widely used, due to its resistant to corrosion and abrasion. Moreover, some properties could be improved using nickel of nanocrystalline instead microcrystalline structure, as nanomaterials exhibit unique physico-chemical characteristics. Furthermore, dispersed hard particles (oxides, carbides) incorporated into a nick-

*   INSTITUTE OF METALLURGY AND MATERIALS SCIENCE, POLISH ACADEMY OF SCIENCES, 30-059 KRAKÓW, 25 REYMONTA STR., POLAND

el deposit can enhance significantly technical parameters of such material, including its mechanical, tribological and anti-corrosion behavior. The inert particles can vary from micrometric to nanometric sizes. Typical diameter of most often used particles are within the range between 1 and 100 μm, but recently the application of ultrafine particles become increasingly important.

Nanocrystalline materials have been mainly produced by inert gas condensation, ball milling, mechanical alloying, mechanochemical processing and electrodeposition. Compared to other methods, electrodeposition, as a low-temperature, cheap and simple method, is a superior technique for preparation of nanocrystalline metals and alloys as well as nanocomposite coatings in a single step without secondary treatment [8,9]. Electrochemical deposition shows also the additional advantages such as high deposition rate, simple equipment, the automation possibility, easy control of microstructure and thickness (from nanometers up to several tens of micrometers) of deposits plated uniformly on substrates of complicated shapes and large surfaces.

During electrodeposition process, insoluble ceramic particles suspended in the multicomponent galvanic bath are embedded in the simultaneously growing metal. The codeposition mechanism for the dispersion of inert particles into metallic coatings is still not entirely understood despite numerous theories presented in literature (e.g. electrophoresis, mechanical entrapment, adsorption and convective-diffusion [2]), due to many factors influencing the electrodeposition process and their interaction. Incorporation of the ceramic particles into a nickel matrix requires the stable suspension in electrolyte, which is difficult to perform especially in the case of nanodispersed phases. Ultrafine ceramic particles show a tendency to agglomerate in the bath due to high surface free energy. Ceramic particles of considerably developed surface form with the electrolyte solution the heterogeneous and thermodynamic unstable binary system, which stability depends mainly on the type, dimensions, concentration and structure of particles as well as on electrolyte parameters.

Over the past decade electrodeposition of Ni-matrix composite coatings has been the subject of numerous investigations. A variety of particles of different size ranging from 4 nm to 100 μm have been incorporated into nickel electrodeposits: e.g. silicon carbide (SiC) [10, 11], cerium dioxide (CeO_2) [12], boron carbide (B_4C) [13], silicon dioxide (SiO_2) [14], silicon nitride (Si_3N_4) [15] titanium dioxide (TiO_2) [16,17], zirconium dioxide (ZrO_2) [18], aluminum dioxide (Al_2O_3) [19-28] and others. One of the most promising materials is the Ni/Al_2O_3 nanocomposite, that can find wide engineering appli-

cation as coatings for engine cylinders, high-pressure valves, car accessories, aircraft microelectronics etc.

The main aim of the present study was to uniformly embedded nano-Al_2O_3 particles into the nanocrystalline nickel matrix by electrochemical deposition from aqueous baths of different composition and to characterize the microstructural and micromechanical properties of obtained Ni/Al_2O_3 coatings.

The influence of embedded non-conducting Al_2O_3 nanoparticles on structure characteristics of the resulting Ni/Al_2O_3 coatings was investigated in order to obtain nanocomposite with high hardness and relatively low residual stresses. As a comparison, the pure Ni coatings were also prepared and characterized under the same conditions.

2. Experimental details

The nickel metallic and Ni/Al_2O_3 nanocomposite coatings were electrochemically deposited in modified low (LC) and high-concentrated (HC) Watt's-type baths into which Al_2O_3 nanopowder (Sigma Aldrich) in amount of 20 g dm^{-3} was added. The pH of the electrolytes was adjusted to 4. For optimized composition of plating solution, the additive EP, consisting of organic compounds mixture was used to reduce both agglomeration of ceramic particles and residual stresses in deposits. The basic chemical composition of the electrolytes used is given in Table 1.

TABLE 1

Chemical composition of the electrolytes of pH 4

Bath number	Concentration [g dm^{-3}]			
	NiSO$_4$·6H$_2$O	NiCl$_2$·6H$_2$O	H$_3$BO$_3$	Al$_2$O$_3$
High-concentrated (HC)				
1	300	50	40	—
2	300	50	40	20
Low-concentrated (LC)				
3	120	70	50	—
4	120	70	50	20
Low-concentrated (LC) with 2.78 g EP additive				
5	120	70	50	20

The electrolysis was carried out in 0.75 dm^3 cell, at room temperature, under galvanostatic regime (3-5 A dm^{-2}), in a system with a rotating disc electrode (RDE). The low-carbon steel cathode of 0.028 dm^2, rotating at 25 rad s^{-1} was supplied by potentiostat/galvanostat PAR 273A. The platinum or nickel sheets (~0.05 dm^2) were used as an anode.

Prior to each experiment, the steel substrates were degreased, chemically polished in solution of oxalic acid and hydrogen peroxide at 35°C and then rinsed in distilled water. The cathode potentials were referred to the saturated calomel electrode (SCE) and were corrected for ohmic drop by the current interupt method (CI). Electrochemical measurements were performed in potentiostatic or potentiodynamic (2 mV s^{-1}) regimes in the potential range from -0.6 V/SCE to -2.2 V/SCE. Before the co-deposition process, the alumina particles were dispersed in the bath using mechanical stirrer (500 rpm) for 24 hours, at room temperature. During last 5 hours, the suspension was extra treated by ultrasounds. In electrodeposition process, additionally to the disk cathode rotating at 25 rad s^{-1}, the intensive mechanical stirring (300 rpm) was employed, in order to maintain the Al$_2$O$_3$ powder in suspension. After electrolysis the samples were ultrasonically cleaned in ethanol for 1 min to remove loosely adsorbed particles from the coating surface and then dried. Mass of deposits was determined by the analytical balance KERN ALT 220-5DAM, with accurate to five points. The coating thicknesses (in the range of 2-35 μm) were estimated on the basis of the deposit weight and the cross-section observations. The surface morphology and cross-section of coatings were examined by scanning electron microscopy (ESEM FEI XL30). Concentrations of elements (Ni, Al, O, Fe) in the electrodeposits were determined using energy-dispersive X-ray spectroscopy (EDS). The cross-section microstructure observations of samples prepared by FIB (Focused Ion Beam) technique were performed by TECNAI G^2 F20-TWIN^{TM} Transmission electron microscope. The phase composition, crystallite size, texture and residual stresses of the deposits were studied by X-ray diffraction technique using CoK$_\alpha$ radiation (diffractometers: Philips PW 1710, Philips X'Pert equipped with texture goniometer ATC3). The crystallite size was evaluated by peak broadening analysis of X-ray diffraction patterns, using the Scherrer equation: $d = \frac{K\lambda}{\beta\cos\theta}$, where d – average crystallite dimension, K – Scherrer constant (assumed as 0.9), λ – the incident radiation wavelength, β – the corrected peak width at half-maximum intensity, θ – angular position. The crystallographic texture of Ni and Ni/Al$_2$O$_3$ layers deposited on the polycrystalline steel substrates was analyzed based on the back-reflection pole figures. The analysis was performed using the orientation distribution function (ODF) calculated by the discrete ADC method from the incomplete pole figures [29]. The residual stresses in coatings were estimated by a sin$^2\psi$ method based on X-ray diffraction data. The hardness of the coatings was measured using a Vickers microindentator (Micro-Hardness Tester CSM Instrument) under an applied load of 200 mN (an average of 10 measurements) in different locations of each coating surface.

3. Results and discussion

3.1. Characterization of the Al$_2$O$_3$ dispersive phase

The commercial Al$_2$O$_3$ powder produced by Sigma Aldrich has been used as original material. XRD and TEM methods were used to characterize the dispersive phase parameters.

3.1.1. XRD technique

The phase composition of Al$_2$O$_3$ powder was analysed by X-ray diffraction using CoK$_\alpha$ radiation in the range of 2θ angle from 15° to 90°. The characteristic XRD pattern shown in Fig. 1 revealed the mixture of the following phases: body-centred monoclinic θ-Al$_2$O$_3$, tetragonal δ-Al$_2$O$_3$ and predominantly face-centred cubic γ-Al$_2$O$_3$.
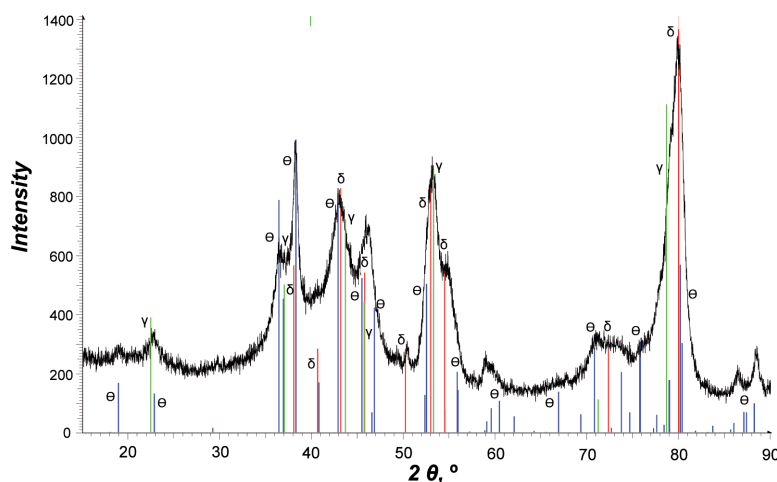

Fig. 1. XRD pattern of the Al$_2$O$_3$ powder (Sigma Aldrich)

3.1.2. TEM technique

TEM microstructure observations show, that Al_2O_3 powder contained the fine needle-shaped crystallites of size definitely below 100 nm and the irregular fraction of crystallites dimension in the range of 20-50 nm (Fig. 2). The average particle size has been estimated as about 30 nm. Electron diffraction patterns of examined powder revealed the presence of the three strong and two weak rings related to the interplanar distance in the range of 0.14-0.28 nm (Table 2). The interplanar distance analysis confirmed predominantly the presence of γ phase and relatively smaller amount of the θ and δ phases. However, similarly to XRD analysis, the α phase of corundum has been excluded.

The impact of ceramic particles in galvanic bath on the electrodeposition process characteristics is ambiguous. Regarding the literature data, it has been found in some cases, that powder suspended in electrolyte solution promotes the higher current densities (depolarization effect) and the $(j - E)$ metal-matrix reduction curves are shifted to the less negative potentials [5, 20-32]. However, in other systems polarization of electrodeposition process is observed [6, 33]. The presence of inert particles could influence the metal deposition process in different way [11]. Incomplete embedding of particles into the growing metal matrix results in apparent decrease of active cathode surface due to the blocking effect. On the other hand, the ceramic nano-particles completely incorporated into nickel matrix could lead to surface development and in consequence to the decrease of effective current density of electrodeposition process.
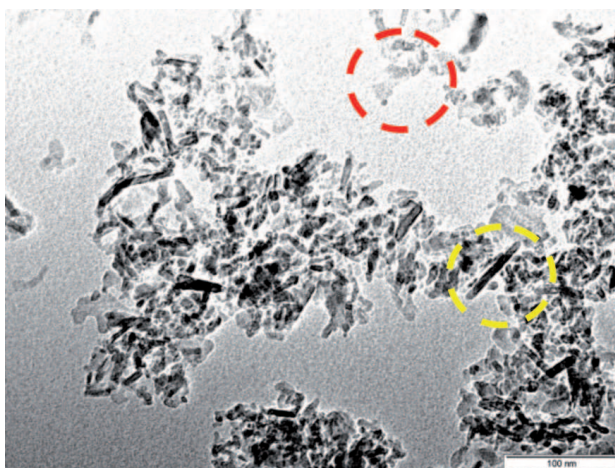

Fig. 2. TEM microstructure of Al_2O_3 powder

TABLE 2

Identification of interplanar distances of γ-Al_2O_3 planes

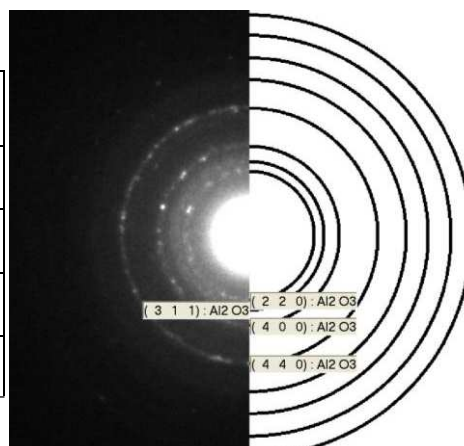| No.	d [Å] measured	d [Å] database	γ-Al_2O_3 planes
1	2.77	2.79	220
2	2.42	2.38	311
3	1.98	1.98	400
4	1.40	1.40	440

Figure 3 shows polarization curves for the steel cathode in the Ni plating solutions of different compositions, with and without Al_2O_3 dispersive phase (Table 1), recorded under potentiodynamic conditions (2 mV s^{-1}) at 25 rad s^{-1} disk rotation speed. Table 3 and Table 4 present respectively: the rate (expressed in cathodic current density) of the nickel electrodeposition process and the current density ratio determined (at selected cathode potentials) in examined electrolyte solutions. As expected, over the whole polarization range, the rate of Ni electrodeposition process from the Ni(II) high-concentrated bath increases (about 1.3 times) compared to the low-concentrated solution.
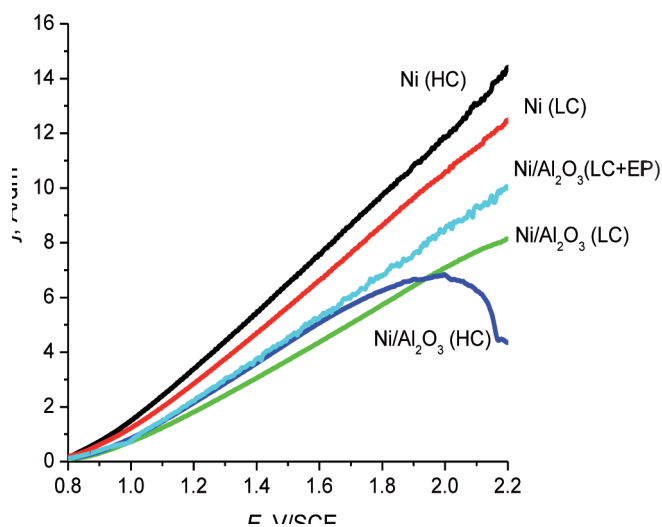

Fig. 3. Global polarization curves recorded under potentiodynamic conditions (2 mV s^{-1}), at 25 rad s^{-1}, in examined solutions of composition given in Table 1

TABLE 3

Ni electrodeposition rate (j), A dm^{-2}

Bath number in Table 1	Bath type	Cathode potential, -V/SCE					
		1.2	1.4	1.6	1.8	2.0	2.2
1	HC	3.66	5.94	8.42	10.97	13.14	16.12
3	LC	2.87	4.69	6.68	8.70	10.61	12.51
2	HC+Al$_2$O$_3$	2.09	3.77	5.23	6.75	7.29	4.69
4	LC+Al$_2$O$_3$	1.86	3.18	4.47	5.90	7.22	8.43
5	LC+Al$_2$O$_3$ +EP additive	2.22	3.76	5.32	6.75	8.5	9.93

The Ni/Al$_2$O$_3$ composite deposition is strongly inhibited in relation to Ni(II) separate discharge, regardless of the nickel concentration in solution. However, this effect is more pronounced for high-concentrated bath (HC), where at the cathode potentials more negative than about -2 V/SCE the electrode surface blocking by

ceramic particles is noticed. For low-concentrated solution (LC), practically constant (about 1.5 times) decrease of the Ni/Al$_2$O$_3$ deposition current density without the blocking effect (as found for the higher Ni(II) concentration in bath) is observed. It is also necessary to take into consideration that the cathode surface was calculated from the geometrical area and the current density was referred to it. Moreover, for the disk working electrode of 18 mm diameter used in the coating electrodeposition, the resistance of the solution (R_s) which depends on specific solution conductivity and cathode area, is substantial and cannot be neglected. The effect of the electrolyte composition on the *IR* potential drop in solutions is shown in Figure 4 and in Table 5 (for the current density of 3 A dm^{-2}). Indeed, due to lower specific conductivity of the suspension compared to the pure Ni(II) bath, for low-concentrated solution containing inert particles the maximum *IR* potential drop (370 mV) was observed. However, the presence of the EP additive (2.78 g dm^{-3}) in that electrolyte (LC) resulted in increase of its conductivity (particle de-agglomeration and promotion of specific cationic adsorption) and the difference in *IR* potential reached value of about 60 mV compared to solution containing only hard ceramic particles.

TABLE 4

The ratio of cathodic current densities

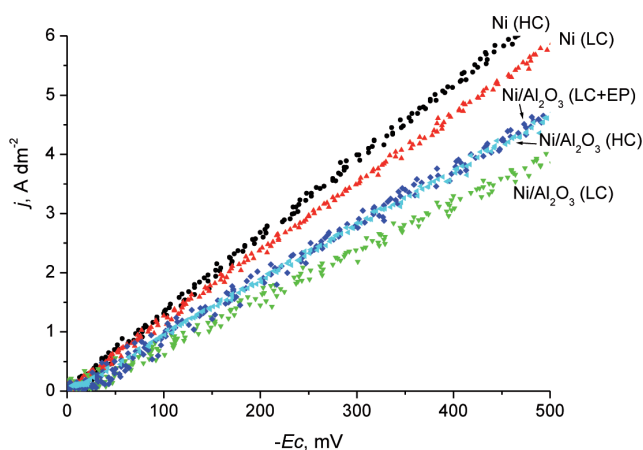| Bath type	Cathode potential, -V/SCE					
	1.2	1.4	1.6	1.8	2.0	2.2
HC/LC	1.3	1.3	1.3	1.3	1.2	1.3
HC/HC+Al$_2$O$_3$	1.8	1.8	1.6	1.6	1.8	3.4
LC/LC+Al$_2$O$_3$	1.5	1.5	1.5	1.5	1.5	1.5
LC/LC+Al$_2$O$_3$ +EP additive	1.3	1.3	1.3	1.3	1.3	1.3

Fig. 4. IR potential drop in examined solutions versus cathode current density

TABLE 5

Deposition potentials, *IR* potential drop and deposition rate of the metallic and composite coatings for the current density of 3 A dm^{-2}

Bath type	Deposition potential, mV/SCE	IR potential drop, mV	Tafel slope, V/decade	Deposition rate	
				mg dm^{-2} s^{-1}	μm dm^{-2} s^{-1}
HC	-1162	-235	0.13	0.84	0.26
LC	-1218	-256	0.12	0.77	0.23
HC+Al$_2$O$_3$	-1322	-317	0.10	0.86	0.34
LC+Al$_2$O$_3$	-1394	-370	0.10	0.90	0.40
LC+Al$_2$O$_3$ + EP additive	-1320	-314	0.10	0.85	0.26

For characterization, the coatings of different thicknesses (in the range of 2-35 μm) were obtained in all examined baths, under galvanostatic conditions (3 A dm^{-2}) at the disk speed of 25 rad s^{-1}. The calculated rate (expressed in mg dm^{-2} s^{-1} and μm dm^{-2} s^{-1}) of Ni/Al$_2$O$_3$ composite deposition was closed and slightly higher than for pure Ni coatings obtained in the same operating conditions (Table 5). The cathodic current efficiency was found to be typical for nickel electrodeposition from Watts bath: 95% – 98.9% for deposition at current density of 3 A dm^{-2} from solutions without particles. In the presence of the Al$_2$O$_3$ phase only a slight decrease in the current efficiency to approximately 90% – 96.5% was observed. Also, the Tafel slopes in the presence and absence of suspended Al$_2$O$_3$ particles were similar (Table 5): 120-130 mV/decade for the pure bath and 100 mV/decade for the bath with particles, the difference is within the range of accuracy of the measurements.

The presence of Al$_2$O$_3$ particles in the electrolytes causes an increase in the cathodic polarization, but the slope is unchanged. The adsorption of particles on cathode surface hinders the deposition of Ni(II), but does not significantly affect the electrochemical reaction mechanism.

3.2. Characterization of coatings

3.2.1. XRD phase analysis and residual stresses

XRD investigations of phase composition and residual stresses of all deposits examined were performed using CoKα filtered radiation. The crystallite size of the coatings was evaluated by peak broadening analysis of X-ray diffraction patterns (Scherrer equation).
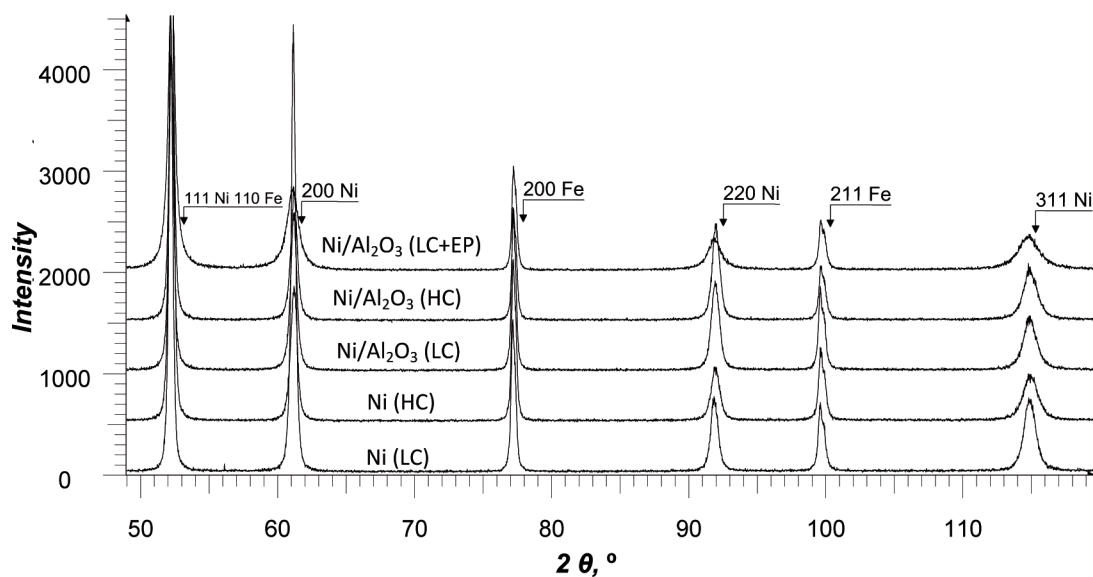

Fig. 5. XRD patterns of Ni and Ni/Al$_2$O$_3$ coatings of thickness about 6 μm obtained from different baths

TABLE 6

Residual stress values of Ni and Ni/Al$_2$O$_3$ coatings

Coating and bath types		Ni (HC)	Ni (LC)	Ni/Al$_2$O$_3$ (HC+Al$_2$O$_3$)	Ni/Al$_2$O$_3$ (LC+Al$_2$O$_3$)	Ni/Al$_2$O$_3$ (LC+Al$_2$O$_3$ + EP additive)
		Residual stress σ_{av}, [MPa]				
Thickness, μm	6	124 ± 35	136 ± 37	120 ± 23	116 ± 24	-370 ± 47
	10	115 ± 23	92 ± 27	93 ± 32	84 ± 34	-238 ± 39

Fig. 5 shows the exemplary XRD patterns of nickel and Ni/Al$_2$O$_3$ coatings produced from LC and HC baths. The XRD patterns of Ni/Al$_2$O$_3$ coatings showed that structure exhibits a nickel matrix at different 2θ angles, no peaks characterized Al$_2$O$_3$ were visible. It is known that a small amount of light elements (low Z) in a heavy-element (high Z) matrix are invisible due to the absorption of the X-ray [34]. In addition, the Al$_2$O$_3$ particles have nanometer sizes hence, extensively broadened diffraction peaks are difficult to observe. On the other hand, the grain size of deposits is strongly influenced by the presence of additive in electroplating bath. The addition of small amount of Al$_2$O$_3$ has considerable effect on the grain refining of nickel deposits. On the basis of XRD reflection line broadening (using the APD program) [35] the Ni crystallite sizes in metallic coatings were evaluated (reference to (200) reflection) to be: 30 nm (LC) and 26 nm (HC).

Addition of Al$_2$O$_3$ particles into nickel matrix virtually does not change the Ni crystallite size in composite coatings obtained from both LC and HC baths. However, in coatings obtained from the low-concentrated (LC) bath with EP additive it was significantly lower – about 13 nm. These results indicated that the addition of hard Al$_2$O$_3$ particles led to decrease in the average Ni crystallite size in Ni coatings obtained from LC bath. It is well known that the grain size of deposits is strongly influenced by the presence of additives in electroplating bath [36]. The important role of additive as a grain refiner is its effect on blocking the surface by formation of complex compounds which increases the frequency of nucleation and decreases the surface diffusion of nickel ions adsorbed on cathode surface, and hence retards the crystallite growth [37].

X-ray diffraction plays a prominent role among non-destructive methods for determination of residual stresses in materials. Values of residual stresses of examined coatings were calculated for 220 plane (2θ = 91.8°) regarding the diffraction elastic constants [38] by the Reuss model using a computer program Stress [39]. Evaluated residual stresses are mean values for the volume defined by the cross section of X-ray beam and by the penetration depth of the used radiation. The stresses have been calculated by $\sin^2\psi$ procedure [38]. Table 6 presents stress values determined for coatings (with thickness of 6 and 10 μm) electrodeposited from different baths.

The values of tensile stresses estimated in the coatings electrodeposited from LC and HC solutions of thickness 6 μm were at level of about 120 MPa, however in the coatings of thickness 10 μm they were lower (100 MPa). Additionally, the coatings containing Al$_2$O$_3$ particles were characterized by insignificantly lower values (within limits of error) of residual stress than these without ceramic particles. This relation was observed for both investigated baths LC and HC. The Ni/Al$_2$O$_3$ deposits obtained from LC solution with 2.78 g EP additive were found to possess compressive residual stresses, which values diminished with increasing coating thickness.

3.2.2. Texture

The pure electroplated nickel films frequently revealed a fibre texture of different components: <100> (observed the most frequently), <110>, <210>, <111>, <211> depending on plating conditions, mainly pH and current density of metallic deposition [22,27,40]. The textural developments are usually attributed to the existence or formation of different chemical species during the cathodic process [41]. Molecular or atomic hydrogen as well as hydroxyl groups adsorbed on the cathode predominantly act as inhibitors and selectively promote the growth in different crystallographic directions [27, 41]. Texture of examined Ni and Ni/Al$_2$O$_3$ coatings was analysed using the orientation distribution functions (ODF) calculated by the discrete ADC method [29] from the incomplete pole figures measured using X-ray diffraction. Analysis of pole figures and orientation distribution functions revealed occurrence of strong {210}<uvw> fibre texture component in all examined coatings. The {100}<uvw> texture was observed only in the Ni electrodeposited from LC bath. In examined samples the codeposited Al$_2$O$_3$ particles have not influenced the preferred growth orientations for Ni grains. However, the Ni/Al$_2$O$_3$ coating obtained from LC solution

with EP additive exhibited the most diverse texture of all and it also revealed {110}<uvw> fibre texture beside mentioned above. Figure 6 presents created 3D plots of the characteristic ODF sections (for $\phi_2 = 0$) [42].
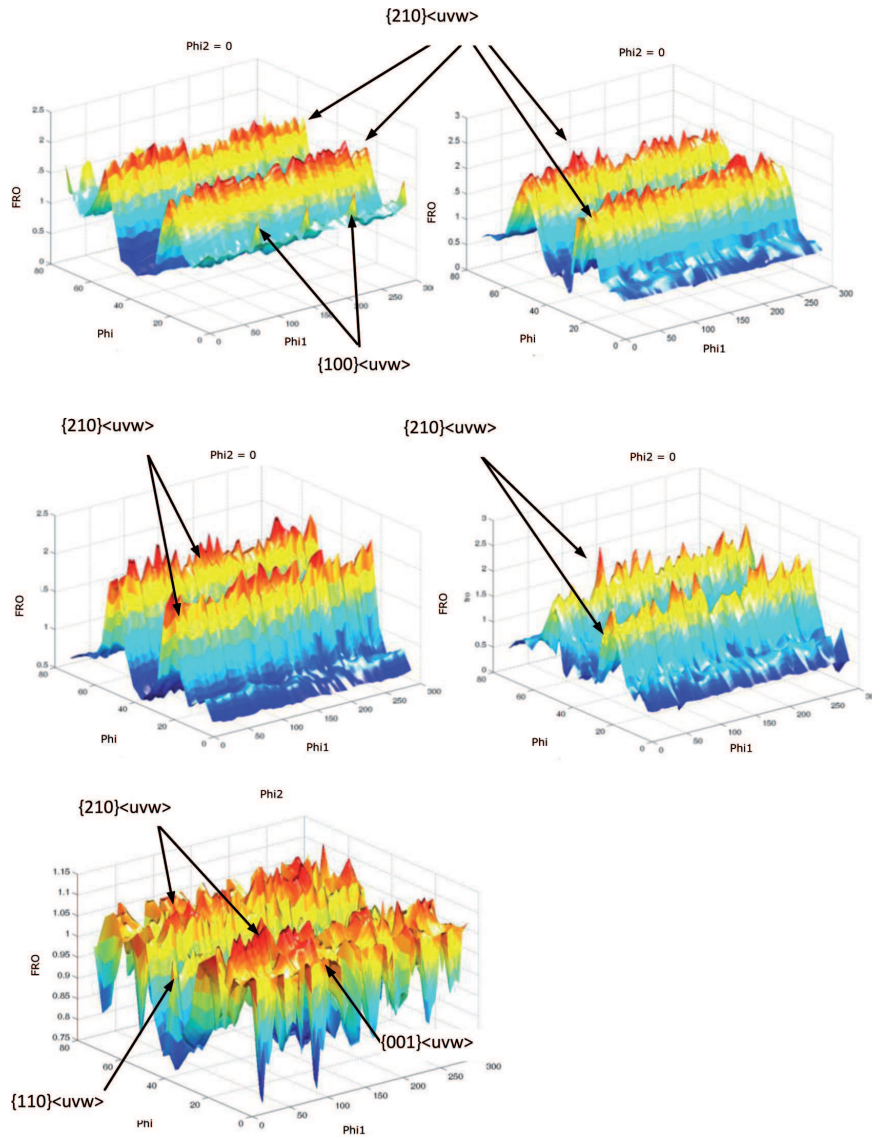

Fig. 6. ODF sections (for $\phi_2 = 0$) of Ni and Ni/Al$_2$O$_3$ deposits (thickness of 6 μm): a) Ni (LC), b) Ni/Al$_2$O$_3$ (LC), c) Ni (HC), d) Ni/Al$_2$O$_3$ (HC), e) Ni/Al$_2$O$_3$ (LC with 2.78 g EP additive)
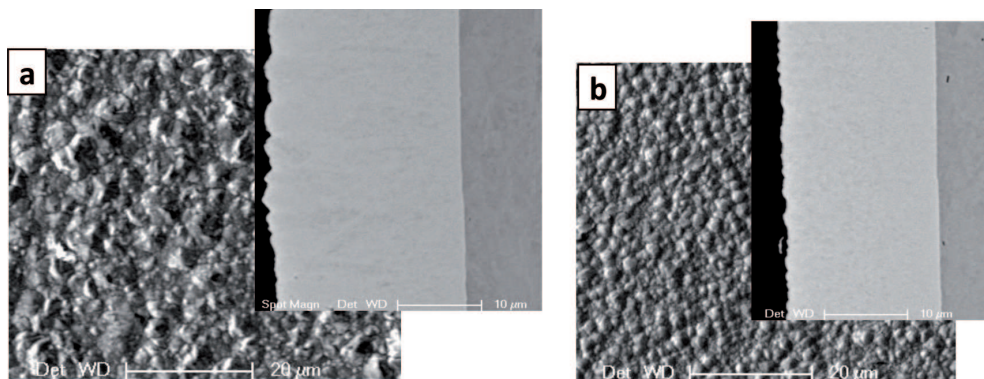
Fig. 7. SEM (secondary electron) image of surface and cross-section of Ni coatings deposited from high-concentrated (a) and low-concentrated (b) baths

3.2.3. Microstructure

Figure 7 presents the SEM images of surface and cross-section of metallic nickel coatings electrodeposited from both examined solutions (HC and LC). A regular pyramidal structure was observed at the surface of the nickel coatings, especially for Ni (HC) (Fig. 7a). As seen, the average dimension of the pyramids on the surface of Ni coatings obtained from solution of lower Ni(II) concentration is substantially reduced, resulting in more regular morphology and a smaller surface roughness grade (Fig. 7b). The cross-section SEM images revealed the all coatings were well adhered to the steel substrate.

The addition of γ-alumina nanoparticles (20 g dm^{-3}) into nickel plating baths (HC and LC) resulting in the significantly changes in the surface morphology of the composite coatings. Figure 8 exemplifies the element concentration distribution along the line presented in SEM image of obtained Ni/Al$_2$O$_3$ coating.

Figure 9 compares the surface of the composite deposits produced in the both type of baths. As seen, the typical pyramidal morphology of nickel deposits from additive-free baths (Fig. 7) has changed into greatly refined (spherical) globular microstructure. The same effect related to the change from preferred orientation to random oriented composite deposits was observed for the nickel coatings with SiC nanoparicles [43]. Moreover, the Ni/Al$_2$O$_3$ composite coatings (Fig. 9b) electrodeposited from low-concentrated solution (bath no. 4, Table 1) are more fine, compact and uniform than that of the HC nickel deposits (Fig. 9a). The similar ionic strength effect of the solution on the particle agglomeration was observed for Ni/Al$_2$O$_3$ deposited from sulfamate bath [24].
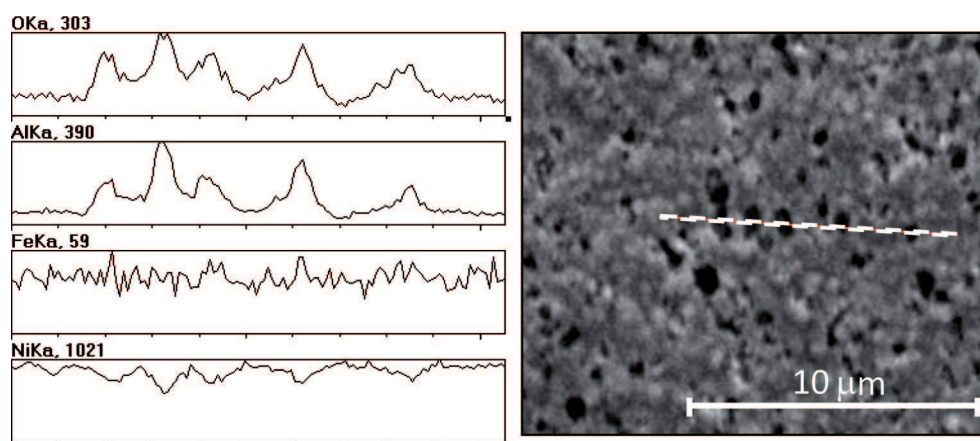

Fig. 8. Element distribution (linescan) of exampled Ni/Al$_2$O$_3$ composite coating electrodeposited from HC solution
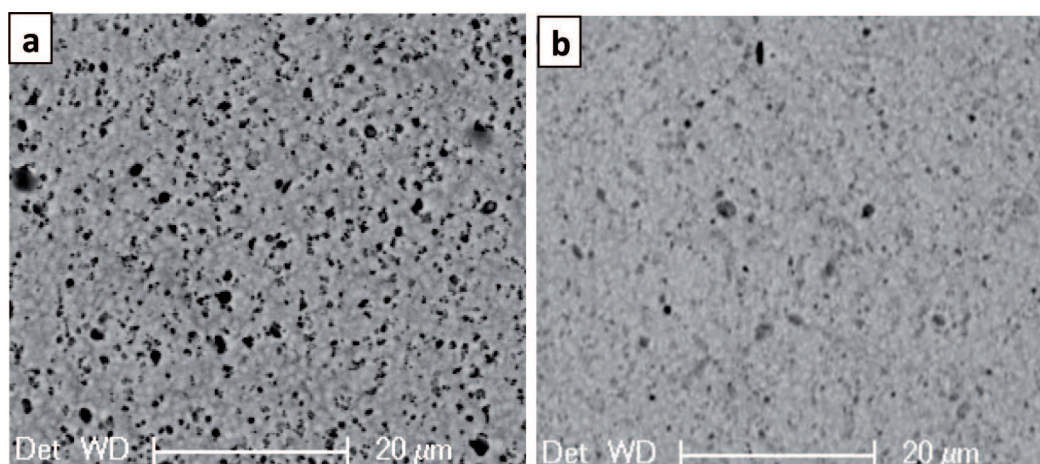

Fig. 9. SEM backscattered electron image of surface of Ni/Al$_2$O$_3$ coatings deposited from high-concentrated (a) and low-concentrated (b) baths
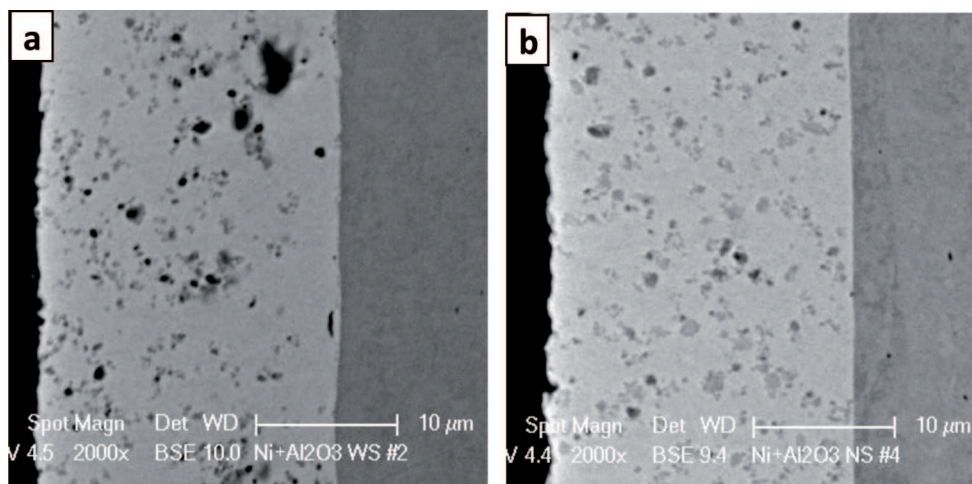
Fig. 10. The cross-sectional morphology of Ni/Al$_2$O$_3$ electrodeposited from high-concentrated (a) and low-concentrated (b) baths
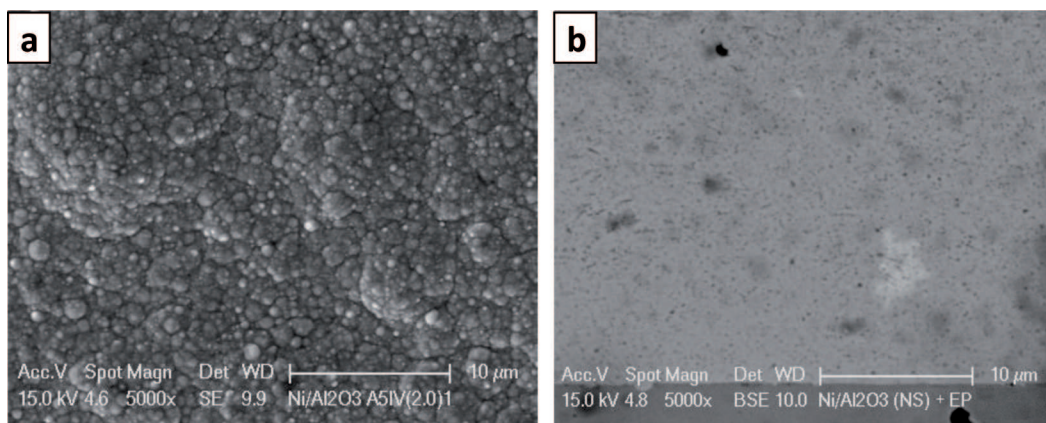

Fig. 11. SEM image of surface and cross-section of composite coatings deposited from bath with organic additions (bath no. 5, Table 1)

The SEM backscattered electron images of cross-section of nanocomposite Ni/Al$_2$O$_3$ coatings electrodeposited from HC an LC solutions are shown in Figure 10. As seen the Al$_2$O$_3$ particles (in dark contrast) are more homogeneously dispersed in the volume of composite deposit obtained in low-concentrated solution (Fig. 10b) compared to HC bath, although some of them formed agglomerated clusters. Moreover, these coatings are characterized by a smoother surface morphology. Hence, it was adopted that the low-concentrated bath is most attractive for further optimization of particle dispersion.

The introduction of the EP surfactant into low-concentrated bath led to de-agglomeration of nano-alumina particles as seen in Fig. 11, in which SEM images of surface and cross-section of composite coatings deposited from bath with organic additions are presented.

The chemical composition of Ni/Al$_2$O$_3$ composites electrodeposited from different electrolyte solutions was determined by EDS technique (Table 7). The embedded weight percentage (wt. %) of Al$_2$O$_3$ in the composite was found to be comparable within all investigated type of coatings.

TABLE 7

Ceramic phase content in Ni/Al$_2$O$_3$ electrodeposits obtained in different solutions

Coating and bath types	Al$_2$O$_3$ content, wt. %
Ni/Al$_2$O$_3$ (HC+Al$_2$O$_3$)	1.3 ± 0.1
Ni/Al$_2$O$_3$ (LC+Al$_2$O$_3$)	1.0 ± 0.1
Ni/Al$_2$O$_3$ (LC+Al$_2$O$_3$ + EP additive)	0.9 ± 0.1

The microstructure of the Ni/Al$_2$O$_3$ composites obtained in pure low-concentrated bath and containing EP additive was examined by TEM technique (Fig. 12). As seen a noticeable difference between the microstructures was observed.
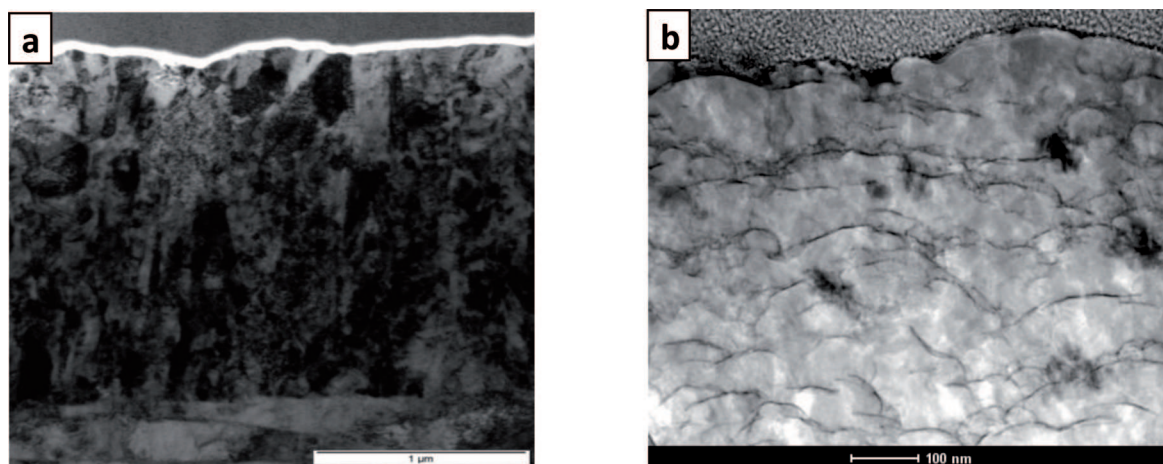
Fig. 12. TEM images of Ni/Al$_2$O$_3$ composites electrodeposited from low-concentrated solution containing 20 g dm^{-3} γ-alumina without (a) and with EP addition (b) respectively

The Ni/Al$_2$O$_3$ composites deposited from solution without the surfactant addition are characterized by uniform microstructure consisting of submicron crystallites with a tendency to columnar growth, similar to pure metallic nickel coatings. Introduction of the EP additive into LC bath caused substantial change in the growth character of coatings (decay of columnar growth), the microstructural refinement of the Ni matrix and uniformity of distribution of oxide particles. The roughness of deposits was in range from 100 to 200 nm.

3.2.4. Microhardness

The influence of fine, hard Al$_2$O$_3$ particles on microhardness values of coating is significant. It was shown that microhardness of the obtained materials exceeded 300 HV for the Ni metallic and 500 HV for Ni/Al$_2$O$_3$ composite coatings (examined by Vickers technique). The incorporated Al$_2$O$_3$ particles significantly increased the hardness of Ni coatings. The improvement in the hardness of composite coatings is probably related to the dispersion hardening effect caused by Al$_2$O$_3$ particles in the composite matrix, which obstructs the shift of dislocation in nickel matrix [28,44]. However, the expected effect of the coating microhardness increase by the presence of the EP additive in the bath has not been observed, despite of the crystallite size reduction, more uniformly distribution of ceramic particles and change from tensile to compressive residual stresses. This effect is probably related to the EP concentration (too high) in the plating bath.

4. Conclusions

Ni/Al$_2$O$_3$ composite electrodeposition under forced convection conditions, from weakly acid sulfate-chloride

solutions on steel substrate, was investigated in order to improve the coating mechanical properties. For comparison, pure nickel coatings obtained under the same electrodeposition conditions were also examined. Polarization studies revealed that the Ni/Al$_2$O$_3$ composite deposition is strongly inhibited in relation to Ni(II) separate discharge, regardless of the electroactive species concentration in the solution. However, this effect becomes more pronounced with increasing of the nickel salt concentration in bath, where the electrode surface blocking by ceramic particles is observed. Generally, the presence of Al$_2$O$_3$ in the electrolytes hinders the deposition of Ni(II) mainly due to the adsorption of ceramic particles on cathode surface and lower specific conductivity of the solutions. It was shown that the non-conducting particles codeposited with the nickel matrix do not significantly affect the electrochemical reaction mechanism, since the slope of the determined cathodic polarization curves remains unchanged. It is well known that functional properties of electrodeposited composites are mainly controlled by their composition and microstructure. During co-deposition, the higher nucleation due to nanoparticles incorporation perturbs the growth of nickel matrix and results in a smaller grain size. Also, due to absorption of Al$_2$O$_3$ on the cathode surface, it increases cathodic polarization and contributes to developing fine grains. The addition of alumina nanoparticles into nickel plating baths also leads to significantly changes in the surface morphology of the composite coatings. The microstructure of the Ni/Al$_2$O$_3$ composite coatings was largely improved, more fine, compact and uniform than that of the pure nickel deposits. The Al$_2$O$_3$ distribution in the nickel matrix, especially obtained in high concentrated bath, was approximately uniform; however, a tendency to agglomeration has been observed. Although a lower concentration of electroactive species tends to

930

favour well-dispersed and less agglomerated nanoparticles. The properties of composite coatings depend mainly on the size and content of the codeposited particles but also on distribution of the particles in the metallic matrix. The influence of the electroactive species concentration and the presence of the surfactant additive consisting of the organic compound mixture (wetting, anti-stress, smooting agents in adequate proportions) on the dispersion of codeposited ceramic particles were determined. The presence of surface-active agents caused (under investigated experimental conditions) a lowering of overpotential of nickel ion reduction. Changes in kinetics of the nickel ions reduction from examined baths containing additive caused an increase of the electrochemical reaction rate versus this rate for a bath without additives. It was found that surface morphology and microstructure are strongly influenced by the additive. The substantial changes in the growth character of coatings (decay of columnar growth), the further microstructural refinement of the Ni matrix and uniformity of distribution of oxide particles have been observed. Compared to coatings electrodeposited from additive free solutions, which revealed the tensile residual stresses, the Ni/Al_2O_3 deposits obtained from bath with surfactant were found to possess compressive residual stresses, which values diminished with increasing coating thickness. The all electrodeposited Ni and Ni/Al_2O_3 coatings were compact and well adhered to the steel substrate. The results indicate that the electrodeposited nanocomposite coatings with uniformly dispersed nano-particles Al_2O_3 in the nickel matrix could be obtained by use a suitable surfactant addition. The composite coatings obtained in these conditions have a more uniform and fine surface microstructure. It has been shown that agglomeration of Al_2O_3 nanoparticles can be reduced also by using a lower concentration of nickel ions solutions. It has been firmly established that the preliminary stage of preparation of suspension in electrolyte solution is crucial for MMC plating as Al_2O_3 nanoparticles aggregate easily in the bath. Applying surfactant addition and ultrasound could efficiently improve the dispersion.

Acknowledgements

REFERENCES

[1] C. Kerr, D. Barker, F. Walsh, Trans IMF **78**(5), 171-78 (2000).

[2] C.T.J. Low, R.G.A. Wills, F.C. Walsh, Surf Coat Tech **201**, 371-383 (2006).

[3] J. Niedbala, A. Budniok, E. Lagiewka, Thin Solid Films **516**, 6191-6196 (2008).

[4] A. Lozano-Morales, E.J. Podlaha, J. Appl. Electrochem. **38**, 1707-1714 (2008).

[5] P.C. Tulio, I.A. Carlos, J. Appl. Electrochem. **39**, 283-291 (2009).

[6] G. Wu, N. Li, D. Zhou, K. Mitsuo, Surf Coat Tech **176**, 157-164 (2004).

[7] H. Ataee-Esfahani, M.R. Vaezi, L. Nikzad, B. Yazdani, S.K. Sadrnezhaad, J Alloys Comp **484**, 540-544 (2009).

[8] N.S. Qu, D. Zhu, K.C. Chan, W.N. Lei, Surf Coat Tech **168**, 123-128 (2003).

[9] A. Góral, J. Deda, E. Bełtowska-Lehman, B. Major, Arch Metall Mater **53**, 979-984 (2008).

[10] N.K. Shrestha, M. Masuko, T. Saji, Wear **254**, 555-564 (2003).

[11] R.P. Socha, K. Laajalehto, P. Nowak, Colloids and Surfaces A: Physicochemical and Engineering Aspects **208**, 267-275 (2002).

[12] S.T. Aruna, C.N. Bindu, V.E. Selvi, V.K. William Grips, K.S. Rajam, Surf Coat Tech **200**, 6871-6880 (2006).

[13] V. Medelien, Surf Coat Tech **154**, 104-111 (2002).

[14] P. Nowak, R.P. Socha, M. Kaisheva, J. Fransaer, J.P. Celis, Z. Stoinov, J Appl Electrochem **30**, 429-437 (2000).

[15] M. Trzaska, A. Wyszynska, M. Kowalewska, Composites **2**, 338-341 (2002).

[16] A.A. Aal, H.B. Hassan, J Alloys Comp **477**, 652-656 (2009).

[17] M. Zhou, N.R. Tacconi, K. Rajeshwar, J Electroanal Chem **421**, 111-120 (1997).

[18] L. Benea, J Appl Electrochem **39**, 1671-1681 (2009).

[19] Y.S. Dong, P.H. Lin, H.X. Wang, Surf Coat Tech **200** , 3633-3636 (2006).

[20] M. Verelst, J.P. Bonino, M. Brieu, A. Rousset, Mat Sci Eng A-Struct **191**, 165-169 (1995).

[21] J. Steinbach, H. Ferkel, Scripta Mater **44**, 1813-1816 (2001).

[22] T. Lampke, B. Wielage, D. Dietrich, A. Leopold, Appl Surf Sci **253**, 2399-2408 (2006).

[23] B.F. Levin, J.N. DuPond, A.R. Marer, Wear **238**, 160-167 (2000).

[24] S.L. Kuo, Y.Ch. Chen, M.D. Ger, W.H. Hwu, Mater Chem Phys **86**, 5-10 (2004).

[25] A.B. Vidrine, E.J. Podlaha, J Appl Electrochem **31**, 461-468 (2001).

[26] C. Gheorghies, G. Carac, I.V. Stasi, J Optoelectron Adv M **8**, 1234-1237 (2006).

[27] L. Chen, L. Wang, Z.G.J. Zhang, Mat Sci Eng A-Struct **434**, 319-325 (2006).

[28] H. G u l, F. K i l i c, A. A l p, H. A k b u l u t, Wear **267**, 976-990 (2009).

[29] K. P a w l i k, Phys Status Solidi B **134**, 477-483 (1986).

[30] L. B e n e a, P.L. B o n o r a, A. B o r e l l o, S. M a r t e l l i, F. W e n g e r, P. P o n t h o a u x, J Electrochem Soc **148**, C461-C465 (2001).

[31] E.C. L e e, J.W. C h o i, Surf Coat Tech **148**, 234-240 (2001).

[32] R.P. S o c h a, P. N o w a k, K. L a a j a l e h t o, J. V ä y r y n e n, Colloid Surface A **235**, 45-55 (2004).

[33] B. S z e p t y c k a, A. G a j e w s k a, Composites **3**, 23-29 (2003).

[34] B.D. C u l l i t y, Elements of X-ray Diffraction, Addison-Wesley Publishing Co., Inc., London 1959.

[35] Software Operation PC-APD, Philips Analytical X-Ray Customer Support 1989.

[36] D.A. V e r m i l y e a, J. Electrochem. Soc. **109**, 295-301 (1962).

[37] Rashidi, A. Amadeh, Surf Coat Tech **204**, 353-358 (2009).

[38] I.C. N o y a n, J.B. C o h e n, Residual stresses – Measurement by Diffraction and Interpolation. Springer-Verlag, New York, 1987.

[39] A. B a c z m a ń s k i, Program Stressfit, AGH, Krakow, 2004.

[40] M.G. M a u r i n, Contribution a l'etude des depots electrolytiques textures de nickel et de cobalt. PhD Thesis, Zurich, 1970.

[41] J. A m b l a r d, I. E p e l b o i n, M. F r o m e n t, G. M a u r i n, J Appl Electrochem **9** (2), 233-242 (1979).

[42] M. S w i e t e k, Orientation distribution function analysis of crystallites. Computer program creation. MA Thesis (in Polish), Technical Institute UP, Krakow, 2009.

[43] Y. Z h o u, H. Z h a n g, B. Q i a n, Appl Surf Sci **253**, 8335-8339 (2007).

[44] G. W u, N. L i, D. Z h o u, K. M i t s u o, Surf Coat Tech **176**, 157-164 (2004).